Indian Institute of Science Education and Research, Mohali

Masters Thesis

Study of long range correlations in biophotonic architectures

DANISH SHAMOON

A thesis submitted in partial fulfilment of the requirements for the BS-MS dual degree in science

in the

Femtosecond Laser Laboratory, CAF
Department of Physical Sciences, IISER Mohali

April 2014

Declaration of Authorship

I, Danish Shamoon, declare that this thesis titled, 'Study of long range correlations in biophotonic architectures' and the work presented in it are my own. I confirm that:

- This work was done wholly or mainly while in candidature for a research degree at IISER Mohali.
- Where any part of this thesis has previously been submitted for a degree or any other qualification at this University or any other institution, this has been clearly stated.
- Where I have consulted the published work of others, this is always clearly attributed.
- Where I have quoted from the work of others, the source is always given. With the exception of such quotations, this thesis is entirely my own work.
- I have acknowledged all main sources of help.
- Where the thesis is based on work done by myself jointly with others, I have made clear exactly what was done by others and what I have contributed myself.

Signed: _____

Date: _____

Certificate of Examination

This is to certify that the dissertation titled, 'Study of long range correlations in biophotonic architectures' submitted by Danish Shamoon(Reg. No. MS09041) for the partial fulfillment of BS-MS dual degree programme of the Institute, has been examined by the thesis committee duly appointed by the Institute. The committee finds the work done by the candidate satisfactory and recommends that the report be accepted.

Dr. Kamal P. Singh (Supervisor)

Dr. Abhishek Chaudhury

Dr. Ramandeep Singh Johal

"The nature of any process or event belonging to the space-time geometry of the universe has its own ways of revealing itself in the language of human conceptual frameworks when the human begins to reason"

Danish Shamoon

Abstract

The complex spatial arrangements that are found as biophotonic architectures on a termite wing membrane have been observed to scatter a coherent laser beam in a complex manner. This particular behavior has been explored experimentally and numerically in the form of a multivariate analysis with particular sets of variables and an explanation for such behavior with theoretical validation has been presented. A literature survey of closely related topics and some areas of applications have also been highlighted.

Acknowledgements

I am grateful for the unique opportunities, interactions and people that I found while spending time in IISER Mohali during 2009 to 2014. The study had begun as a summer project with Dr. K. P. Singh who introduced this problem to me and also encouraged me to begin using MATLAB. I am grateful to Dr. K. P. Singh as working on this problem step by step, I gained a fruitful experience of learning and a desire to learn more. As a significant amount of work currently presented uses MATLAB in some way or other, so a special thanks also goes to Mathworks, the company that developed this wonderful language.

Dr. Pramod Kumar and Dhirendra Pratap Singh are acknowledged for the associated experimental work. I am grateful to Dr. Pramod Kumar who had been a major player in publishing of the associated results and also presenting it at international conferences.

Aniruddha Dhamorikar, an entemologist whom I contacted through www.allexperts.com deserves special thanks for identifying the insect that was used.

Gopal Verma and Bhupesh Kumar are acknowledged for their help and support in the lab.

Danish Shamoon

Contents

Declaration of Authorship ii

Certificate of Examination iii

Abstract vi

Acknowledgements vii

List of Figures xi

List of Tables xiii

1 Introduction 1
- 1.1 Warm up . . . 1
- 1.2 Introduction to Biophotonics . . . 1
- 1.3 The Approach for addressing the particular problem . . . 3

2 Experimental Results 7
- 2.1 Images of sample . . . 8
- 2.2 Screen distance variation . . . 9
- 2.3 Beam spot radius variation . . . 10
- 2.4 Beam spot position variation . . . 10
- 2.5 Laser source variation . . . 11

3 SEM image analysis 13
- 3.1 Introduction . . . 13
- 3.2 Morphological operations . . . 14
- 3.3 Gaussian masking . . . 15
  - 3.3.1 Mask radius variation . . . 15
  - 3.3.2 Scanning the mask over image . . . 16
- 3.4 Binary or Labeled OBjects (BLOB) analysis . . . 16
  - 3.4.1 Examining distribution of objects' geometric properties . . . 17

3.4.2 Examining the effects of different shapes of objects 19

4 Pattern generation **21**
4.1 Introduction 21
4.1.1 Pattern formation in biological systems 21
4.2 User defined pattern generation 22
4.2.1 2D analogue of N-slit experiment 22
4.2.2 Fluctuations in radius and center 23
4.2.3 Fluctuations in orientation 24
4.2.4 Multiple periodicities in one signal 25

5 Concluding remarks **27**
5.1 Summary and discussion 27
5.2 What more can be done 29
5.3 Possible applications of this study 30

A MATLAB scripts **33**
A.1 For SEM image analysis 33
A.2 For pattern generation 35

Bibliography **41**

List of Figures

1.1 Biophotonic architectures 3
1.2 Stable colourful patterns on insect wings 4
1.3 Using FFT in 2D space for far-field approximation of scattering 5
1.4 Verification of scaling factor and agreement between ODP and power spectrum 6

2.1 Experimental setup 7
2.2 Termite insect and scattering of laser beam due to its wing 7
2.3 Images of sample at various magnifications 8

3.1 SEM image of Termite wing for image processing 13
3.2 Gaussian masked SEM images 15
3.3 Spatial distribution of orientation of objects 17
3.4 Histogram for orientation of objects 17
3.5 Histograms for various geometric properties of the objects 18
3.6 Objects having near zero orientation and the circular ones 18

4.1 Many periodicities in one arrangement 25

List of Tables

2.1 Results for screen distance variation 9
2.2 Results for beam spot radius variation 10
2.3 Results for beam spot position variation 11
2.4 Results for laser source variation 12

3.1 Results for morphological operations 14
3.2 Power spectra for various radii of the mask 15
3.3 Power spectra for scanning the mask over image 16
3.4 Power spectra for various shapes on extracted coordinates (a) 19

4.1 2D analogue of N-slit experiment 22
4.2 Size and interspacing distribution variation 23
4.3 Orientation distribution variation 24

5.1 Power spectra for various shapes on extracted coordinates (b) 31

For the spirit of learning in all of us

Chapter 1

Introduction

1.1 Warm up

This study attempts to explain a natural process and explore some of its associated processes using the jargon of many disciplines like biophotonics, signal processing, pattern generation algorithms, mathematics and numerical methods.

So far, in learning and exploring the dazzling mysteries of this universe we know that processes occur at all length scales within or beyond our reach. Be it the atomic scale or the cosmic scale, interactions exist among various groups of various entities at various levels. The motivation for this study was the observed scattering pattern of a laser beam (Figure 2.2) when it passes through a wing of an insect. The pattern on the screen is a consequence of the wave-matter interaction. Hence, a variety of methods that can account for this particular behavior are employed and a general framework of concepts to which it belongs is developed.

1.2 Introduction to Biophotonics

Biophotonic architectures consist of several hundreds or thousands of 'objects' not necessarily identical, in a complex arrangement (a quasi-periodic spatial arrangement, full characterization of which is not necessarily understood) [1], [2], [3], [4]. The complex

networks of 'objects' found in biological organisms are in general multifunctional [5]. The interaction of light with these complex arrangements and its possible use by the living organism is just one aspect in the manifold of its functions. The designs found in biophotonic architectures have evolved through ages to acheive the amazingly efficient and smart present state which even the best artificial designs today cannot possess. This is why biomimetics is a booming research area today [6] as more and more engineers and scientists are beginning to understand and exploit some aspects of these smart natural designs in various applications.

The particular problem that I wish to study belongs to a particular class of problems that have been explored experimentally to some extent [7] in as early as 1970s and theoretical models also proposed around the same period using mathematical justifications dating back to 1930s (Wiener-Kitchine Theorem). However, due to the diversity in observed quasi-periodic natural arrangements getting even wider today with latest imaging techniques, the problem apart from the optical functionality, i.e. purely the emergence of spatio-temporal pattern in nature itself is a growing research area. So, the particular problem that is the subject of this study is the phase modulation of the light in far-field as a result of its interaction with biophotonic architectures.

Wave-matter interaction at a length scale comparable to the scale of the wavelengths present in the incident wave results in the modulation of the emerging (either transmitted or reflected) wave in a wide variety of ways. The simplest set of examples is the far-field diffraction pattern of a single slit, a double slit or an N-slit experiment. A rather complex illustration for visible monochromatic as well as visible band of wavelengths can be found in this study. Studies particular to the colorful patterns can be referred from [4], [5]. (See also Figure 1.1, 1.2 adapted from the same references)

Thus, I attempt to characterize the complex arrangement present in the biophotonic architecture using a simple optical technique and its theoretical validation through this study. It is important to mention that extraction of a similar information otherwise requires the use of SEM or sphisticated live imaging methods.

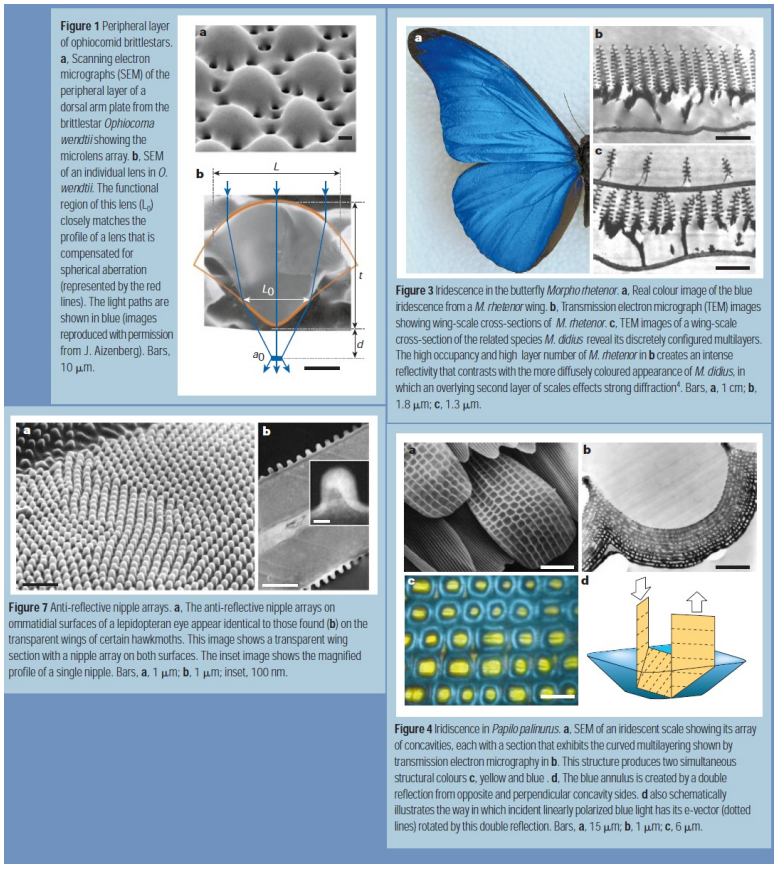

FIGURE 1.1: A variety of biophotonic architectures. For details, see [5]

1.3 The Approach for addressing the particular problem

In order to study the long range structural correlations in biophotonic architectures, I wish to explore and exploit the information in the transmitted complex far-field pattern of the laser beam passing through a transparent wing of a termite species. I also use numerical methods involving image processing and similar tools to address the problems which are difficult to tackle experimentally.

The experimental and numerical results are presented in the form of a multivariate analysis with transmitted intensity distribution in the far-field (in case of experimental result) or the power spectrum (in case of numerical result) being the response variable. The input variables are of two types. One that defines the 2D spatial organization of

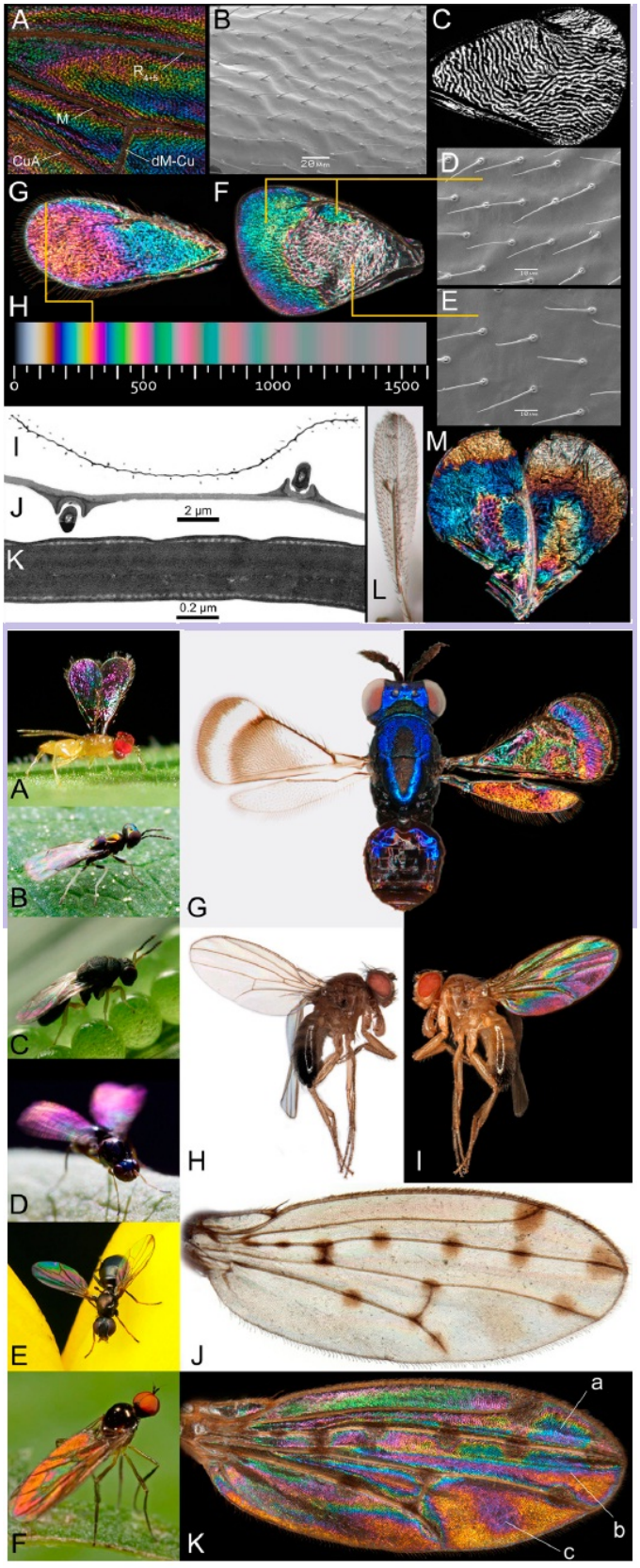

FIGURE 1.2: Stable colourful patterns in insect wings. For details, see [4]

the objects with the identity specific variables which make the sample and the other that are external to the sample. In a multivariate analysis, the input variables are systematically and selectively controlled to examine the response variable. It should be noted that former type of input variables can be easily altered to a much greater extent in a numerical method whereas it can't be easily achieved in experimental method.

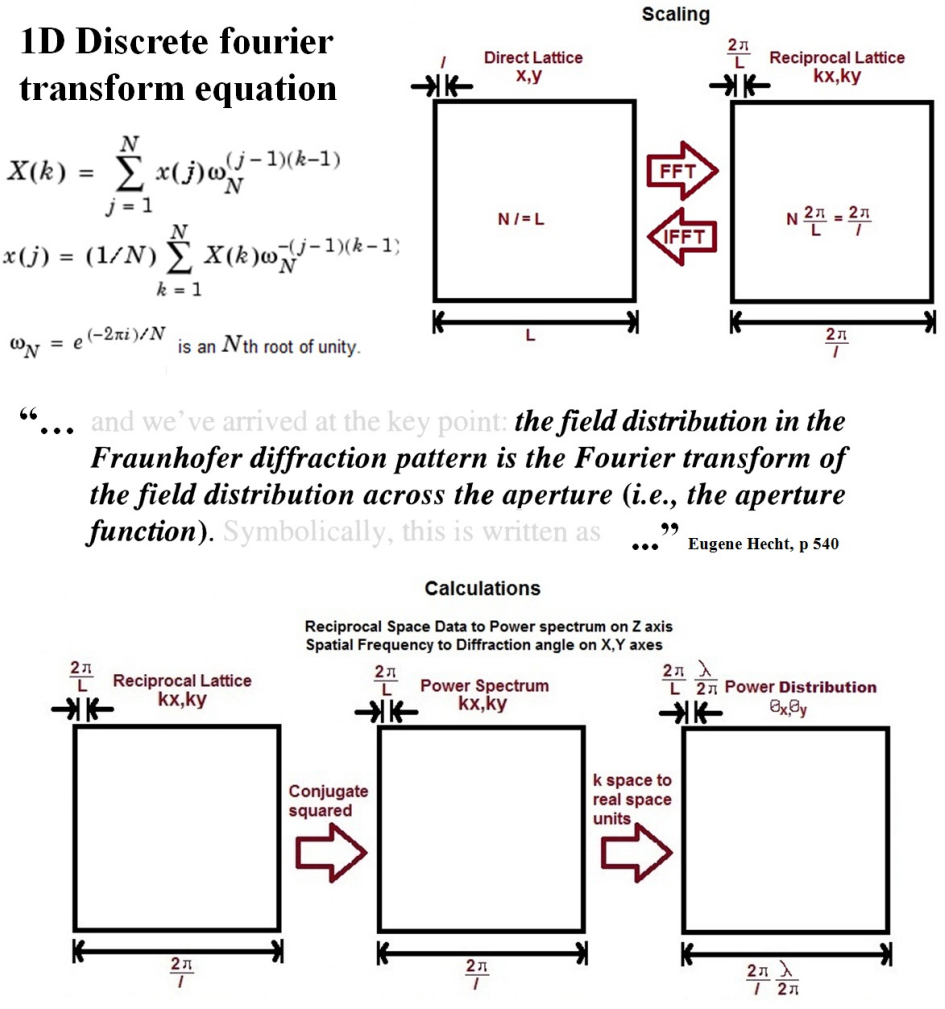

FIGURE 1.3: Using FFT in 2D space for far-field approximation of scattering with associated scaling and calculations

A tool that I repeatedly use in the numerical method is 2D FFT of the sample SEM image or simply some arbitrary binary image generated by varying the input variables.

The theoretical aspects with visualization schemes are shown in the Figure 1.3. The power spectrum calculated from 2D FFT approximates the far-field intensity distribution scattered by a real sample of similar configuration. I demonstrate the close agreement through the Figure 1.4 in which a,c shows the single wire optical diffraction pattern (ODP) and its corresponding intensity cut and b,d shows the power spectrum calculated from the 2D FFT of the microscopic image of the same wire and corresponding intensity cut from the power spectrum. The screen distance units in the ODP have been scaled with a constant derived theoretically.

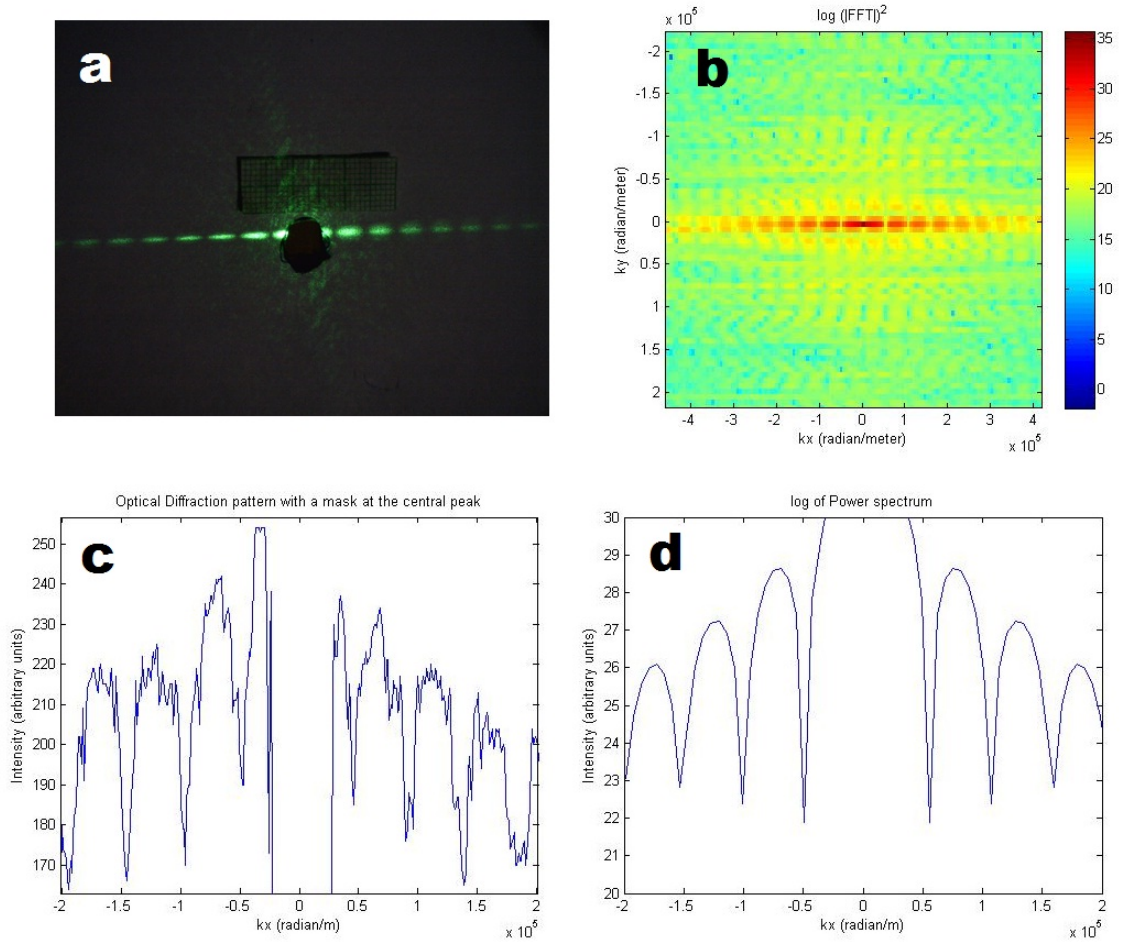

FIGURE 1.4: Verification of the scaling factor and agreement between ODP and power spectrum

Chapter 2

Experimental Results

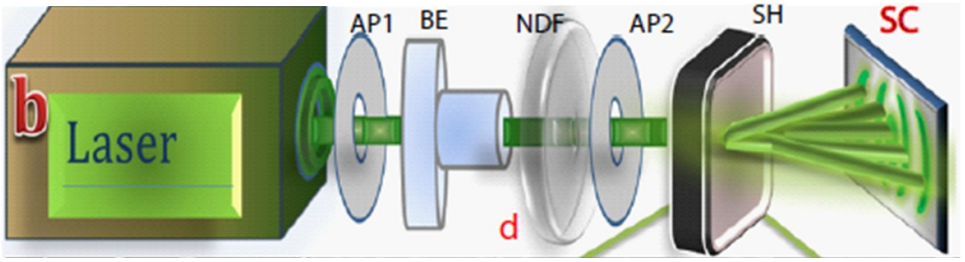

FIGURE 2.1: Schematic of the set-up with various components SH: wing sample holder; AP1,AP2: iris; C: beam expander; SC: screen and NDF: ND filter wheel [8]

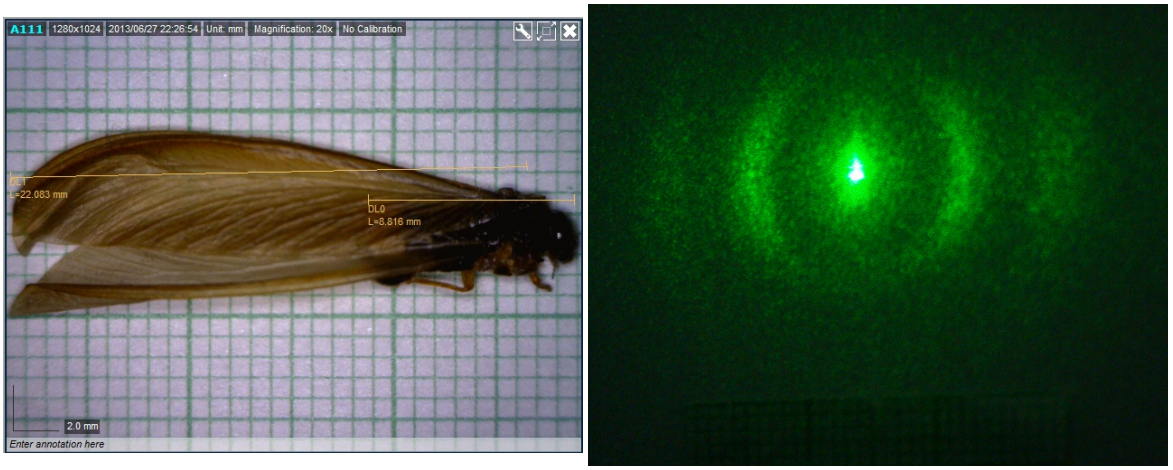

FIGURE 2.2: Left: A Termite species which develops its wings (∼2cm) during the rainy season, otherwise it is wingless. Right: Scattering of green laser beam due to the termite wing. Scale is shown in the image bottom. First lobe is at around 8mm from the central peak. Screen distance is 20.5cm from the sample.

2.1 Images of sample

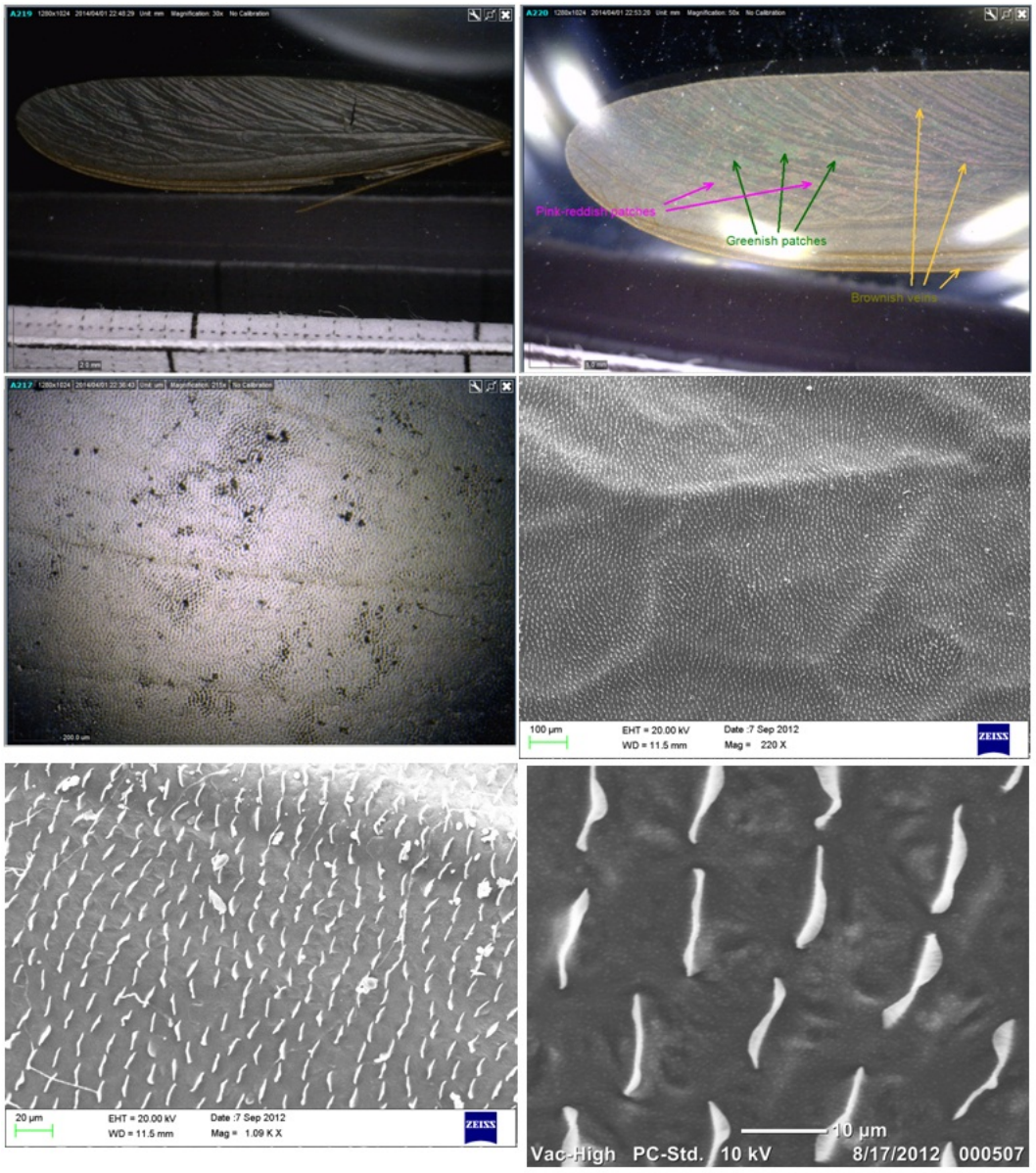

FIGURE 2.3: Images of sample at various magnifications

The images of the termite wing (to be called as sample in the rest of the report) at various magnifications shown in Figure 2.3 provide the first examination of the structural complexity present in it at various length scales. The second picture in the same figure shows the stable colours though faintly visible, similar to the ones shown in Figure 1.2.

2.2 Screen distance variation

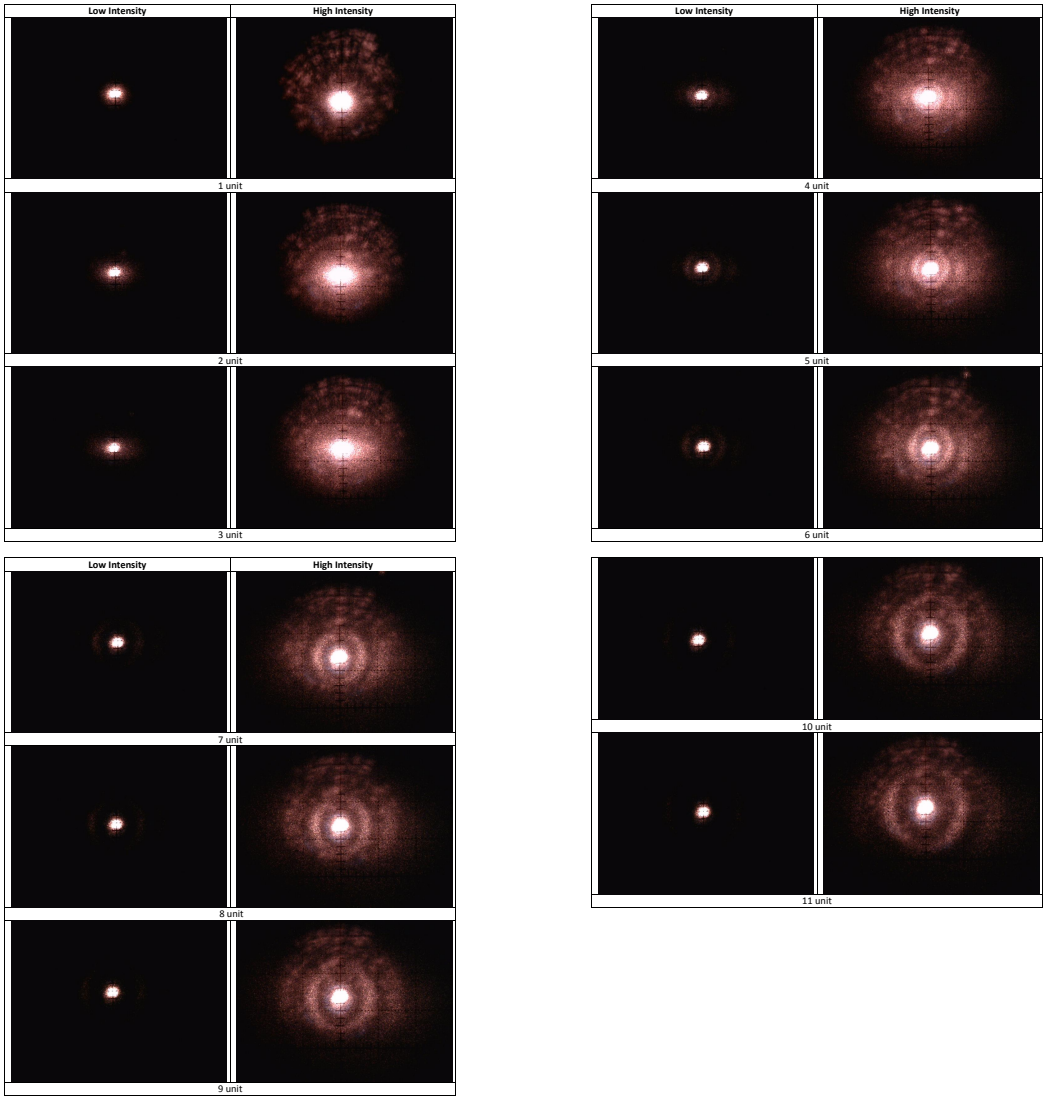

TABLE 2.1: Results for screen distance variation. A unit is equal to an inch and the screen distance from sample is 1cm less than each reading

Within the fixed parameters of the laser, like beam spot size and wavelength, the readings were taken by varying the screen at every inch starting from zero to 11 for low and high intensity of laser source. The characteristic side lobes resolved to the eyes clearly after crossing close to 4 inches from the sample. The result of screen distance variation is simply a diverging intensity distribution. Tracking a point on the first order at all the steps gave a rate of movement 1mm/inch . Extrapolating this rate towards zero suggests that the divergence of this pattern begins right from the

beam spot positioned at the sample and emerging from it. This is probably because the used beam spot was large enough to suppress the characteristic distribution at distances before 4 inches.

2.3 Beam spot radius variation

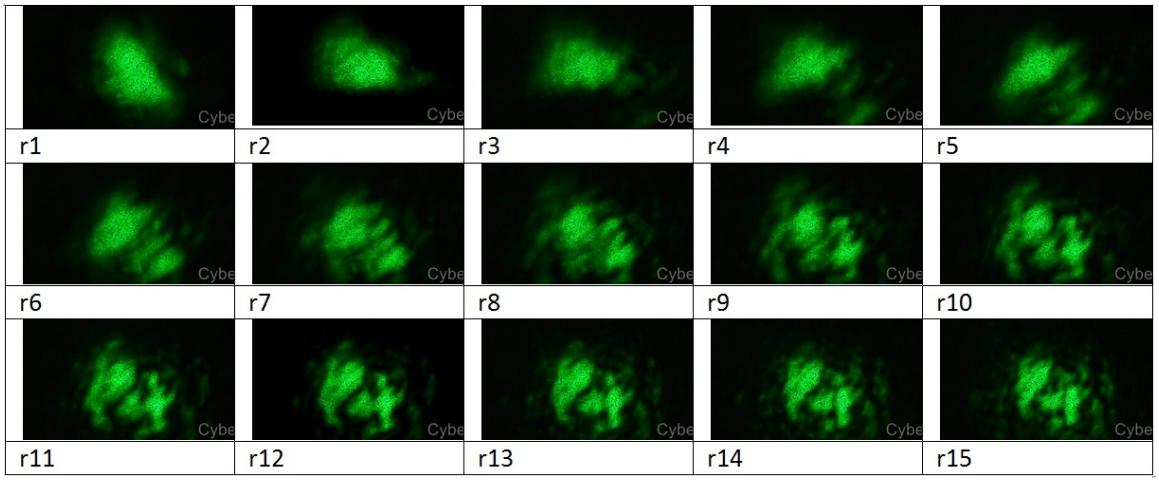

TABLE 2.2: Results for beam spot radius variation. Stepsize is 10 micron (stepsize is for the direction of beam propagation corresponding to which the radius changes according to Rayleigh length formula)

Beam spot radius variation was performed by varying the z axis distance by 10 micron steps near the Rayleigh range of a tightly focused beam at a fixed position of the sample. The beam spot size variation (Figure 2.2) shows the development of the characteristic pattern in its early stages which develops from a very different looking pattern shown at the smallest radius used. However, it must be noted that as the radius further increases and it incorporates more objects, the pattern may still change further.

2.4 Beam spot position variation

Position variation was performed at 5 micron step along x axis for two small radii chosen from the above mentioned experimental data set. The difference between the

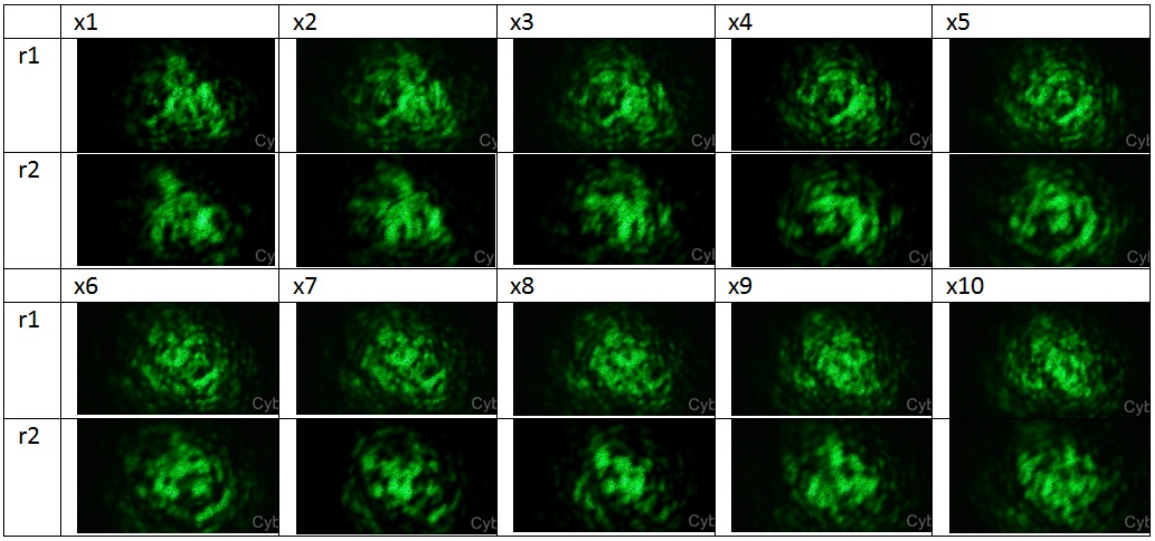

TABLE 2.3: Results for beam spot position variation at different radii. Stepsize is 5μm along x axis.

z axis positions for the two beam spot sizes was 100 micron, r1 being greater than r2. Here as well, the pattern changes in various ways as position under the beam spot is varied.

2.5 Laser source variation

The laser sources were varied in this experiment to check the sensitivity of sample to other wavelengths. This result is adapted from [8]. The only difference in the red (around 630nm) and green (around 530nm) diffraction patterns was a very minute variation in the location of lobes along the radial directions on screen just as it occurs in a single slit experiment with red and green wavelengths. However, the femto-second pulses are short duration and broad band i.e. they contain more wavelengths (centered at 800nm in near IR range). They interacted with the sample in a distinct way giving additional features to the scattering pattern. This experiment is a more advanced topic for this report and can form a separate and interesting study as it may account for time evolution of the observed pattern or allow small modulation of the refractive index of the sample which cannot be done via monochromatic source alone. The different features can be seen in the Figure 2.4.

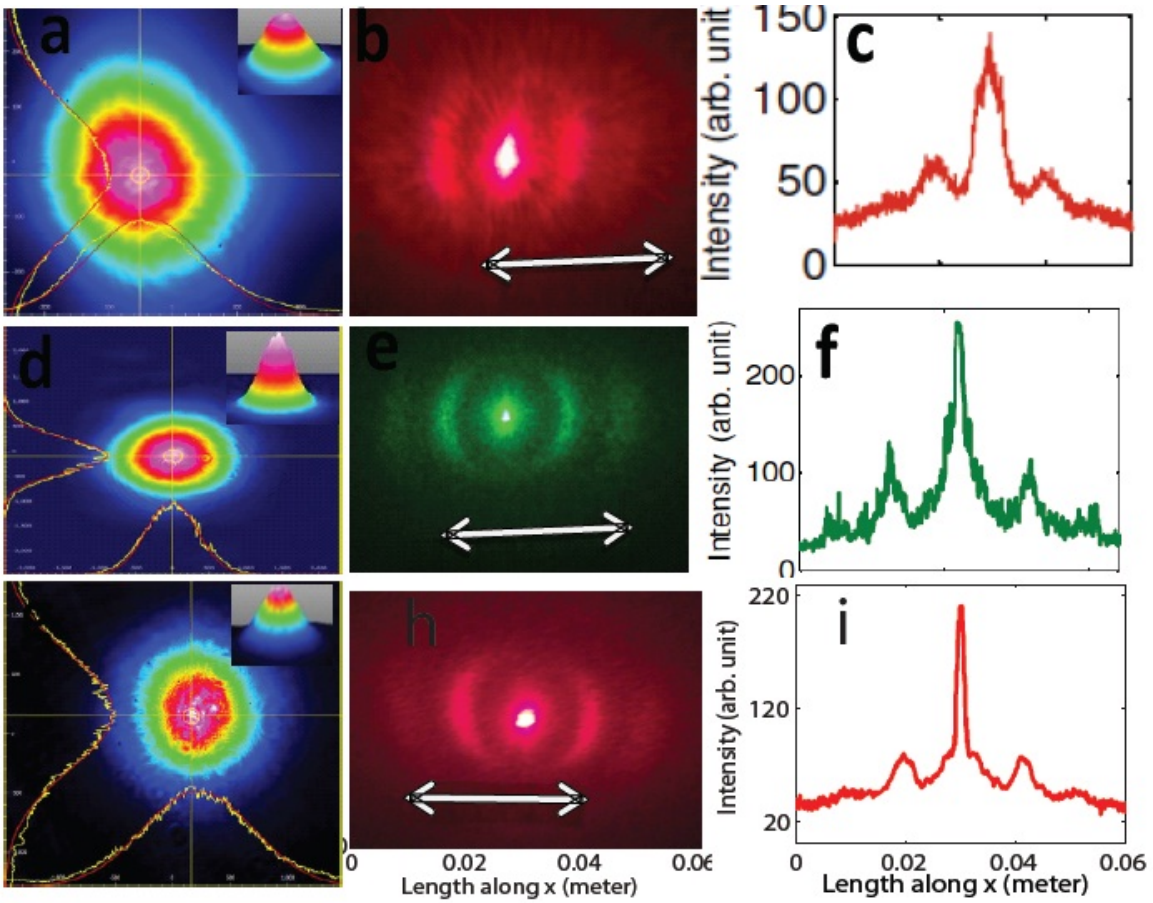

TABLE 2.4: Results for laser source variation. Femto-second pulses (First row), Green laser (Second row) and Red laser (Third row); For details, see [8]

.

Chapter 3

SEM image analysis

3.1 Introduction

The numerical results presented in this chapter are based on the approach of extracting relevant information from the image of the sample by image processing methods. Consequently, the extracted information has been further analyzed. The various methods that I have used are Morphological operations, Image masking and BLOB analysis.

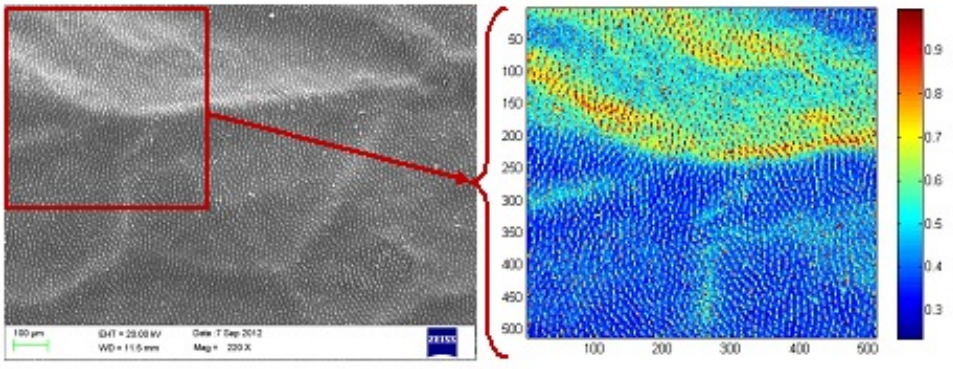

FIGURE 3.1: The image over which the image processing has been carried out. Each pixel corresponds to a square of side 1.2987μm, refered to as dx in this report.

3.2 Morphological operations

In this method, the basic operations are dilation and erosion. With respect to a small reference signal or binary object, dilation induces logical 1 whereas erosion induces logical 0 in the binary image. What it does to the image and its power spectrum is shown in Table 3.1. Some specfic combinations of the two can also be used for extracting the perimeter of the objects. The relevance of using this method and its results in the context of this study is that it facilitates a unique way of shape, size and inter-object distance variation simultaneously that may match with some real spatio-temporal biological patterns. Note that this specific kind of combined variation scheme is different than most of the single variable variation schemes I have employed in this text.

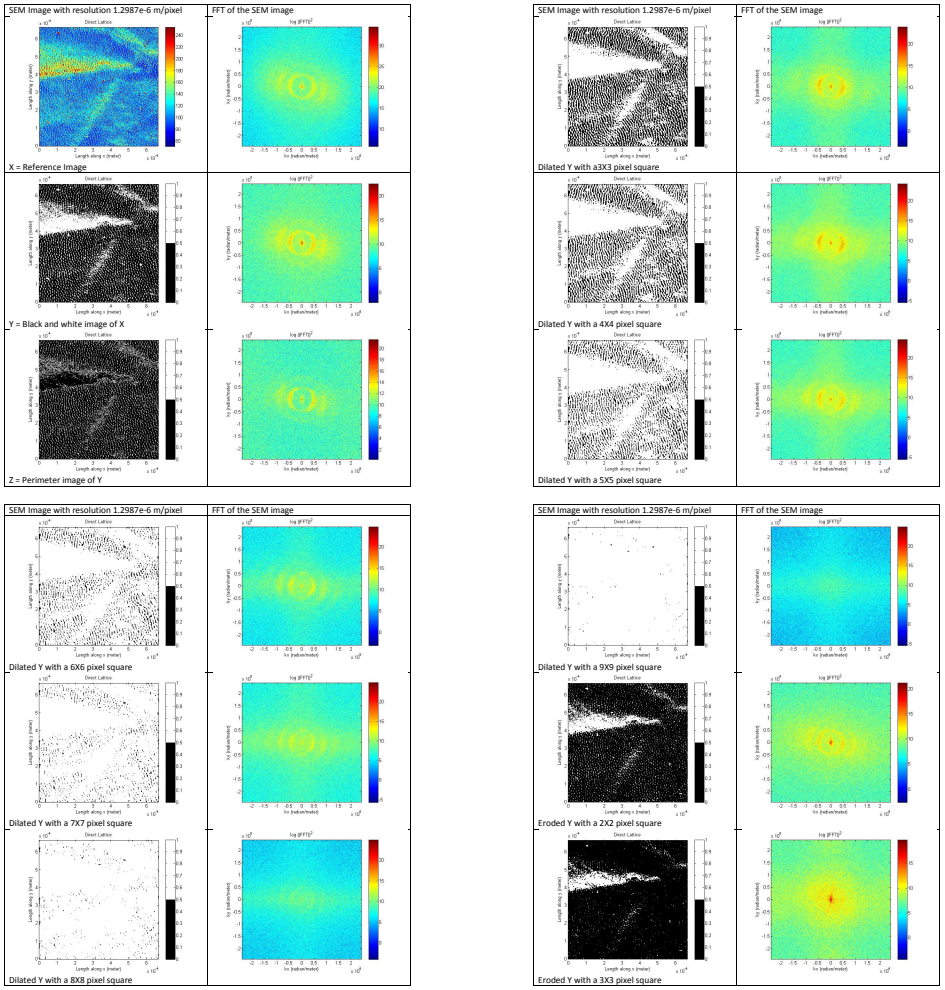

TABLE 3.1: Effects of morphological operations

3.3 Gaussian masking

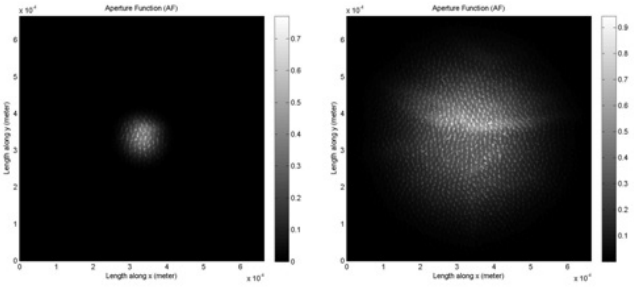

FIGURE 3.2: The radius of the Gaussian mask is 33dx and 123dx respectively.

The image is modulated with a mask in this method as shown in Figure 3.2. A Gaussian mask is chosen here because it creates the effect of an illuminated sample with a laser beam spot. I exploit this method to relate and elaborate the patterns obtained from the experiment using a variable beam spot and scanning over the sample with different sizes of beam spot. This is a theoretical elaboration of the results presented in sections 2.3 and 2.4.

3.3.1 Mask radius variation

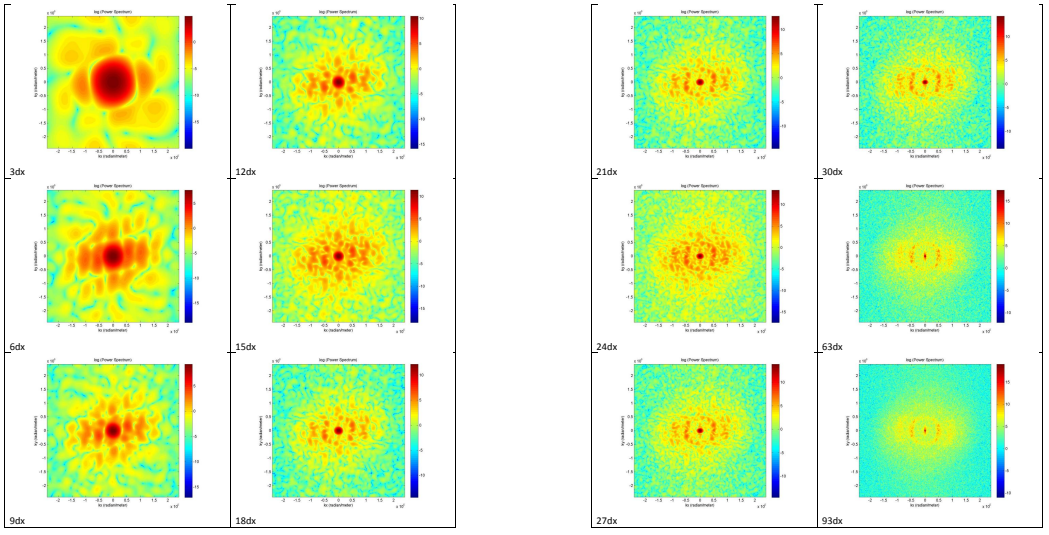

TABLE 3.2: Power spectra for various radii of the mask (Radius mentioned in the left bottom of each cell). Note that the observed pattern begins appearing as early as at 18dx radius

3.3.2 Scanning the mask over image

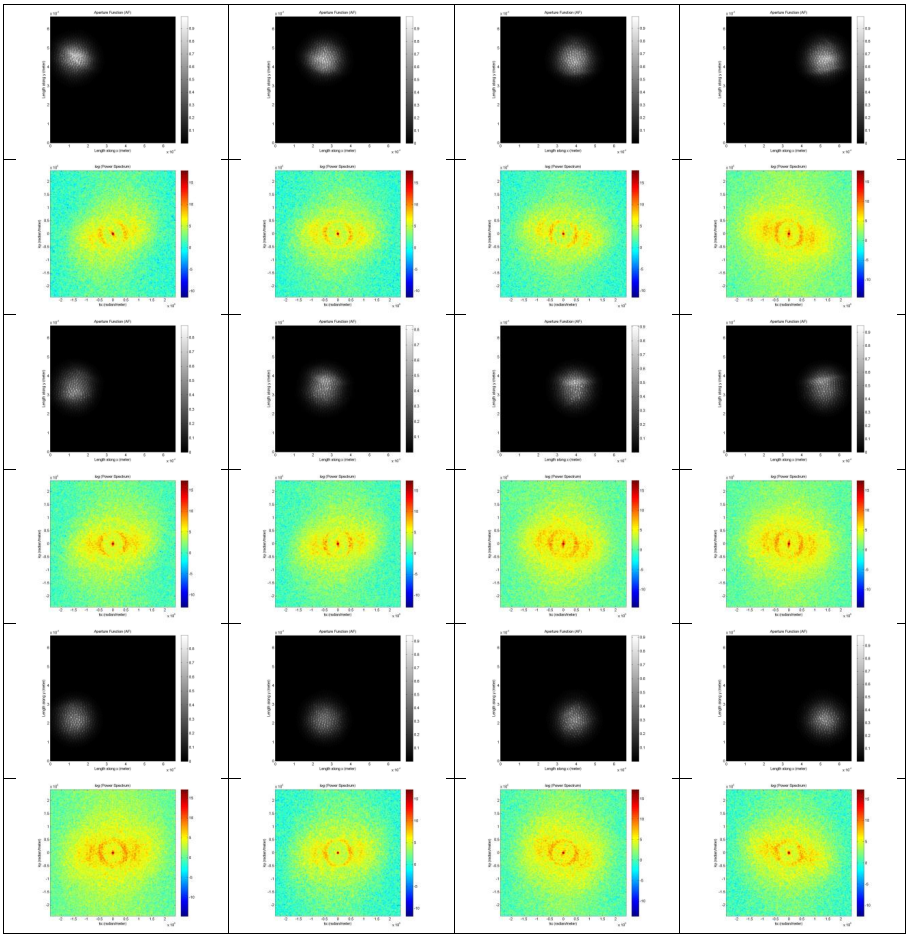

TABLE 3.3: Power spectra for scanning the mask of radius 63dx from left to right starting from 1/3,1/2 and 2/3 of the vertical axis length. Note the changing features in the patterns.

3.4 Binary or Labeled OBjects (BLOB) analysis

BLOB stands for Binary or labeled objects. A binary image is scanned for labeling objects in it based on 8-pixel connectivity. This primarily counts the number of objects labeled as per the connectivity and then various properties of the labeled objects such as centroid coordinates and area can be calculated via inbuilt functions. The objects may also be modeled as ellipses and then calculations for their orientation and lengths of major and minor axes be performed.

3.4.1 Examining distribution of objects' geometric properties

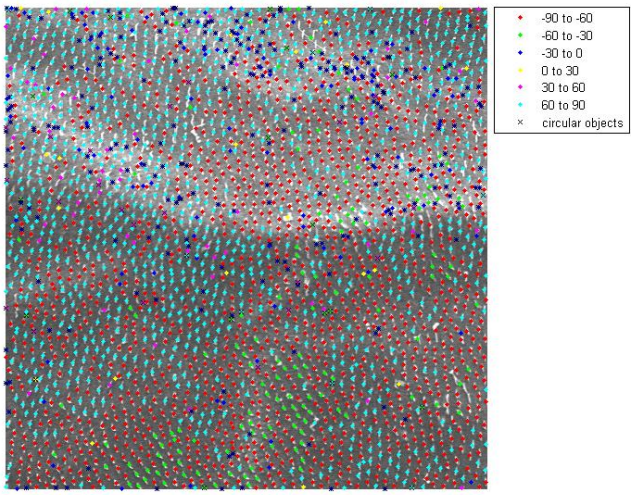

FIGURE 3.3: Spatial distribution of orientation of objects. Open interval for left value and closed interval for right in the legends.

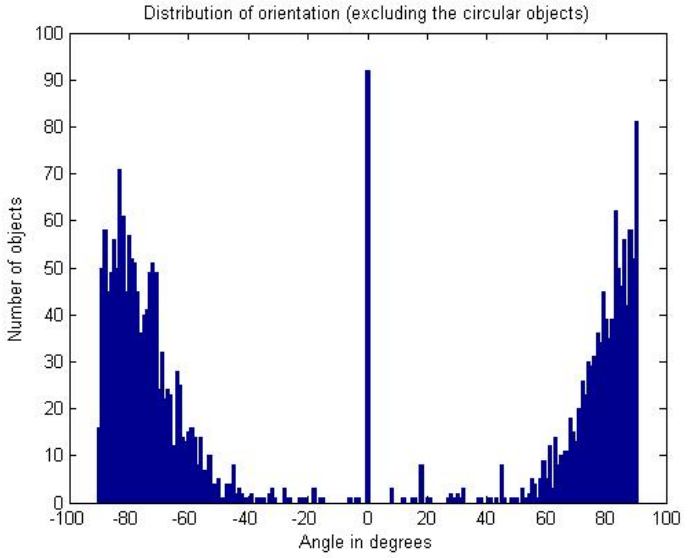

FIGURE 3.4: Histogram for orientation of objects. Central bar mostly corresponds to the incorrect object extraction. The correct number of objects of interest having zero orientation is negligible.

The number of objects counted by the method is 2743 in the cropped SEM image shown in 3.1. It models these objects as ellipses and further calculates the geometric

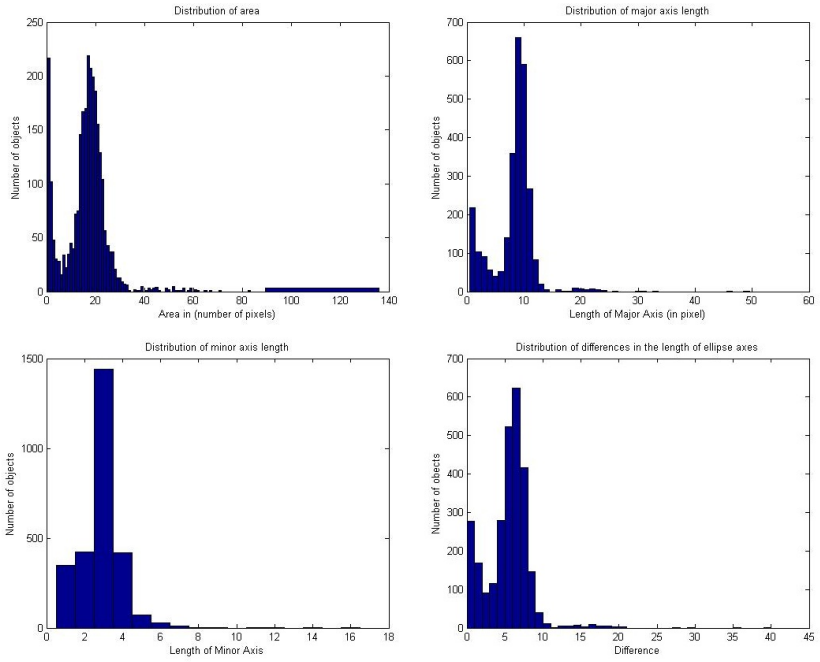

FIGURE 3.5: Histogram for various geometric properties of the objects

properties. Histograms for object properties are also shown in Figure 3.4 and 3.5. It must be noted that the extracted objects are not all correct which is illustrated with the help of Figure 3.6. I call them incorrect objects only in relation to the general objects present in the sample. However, it must be noted that the binary image of the sample highlights all the objects that have a threshold illumination in the SEM image.

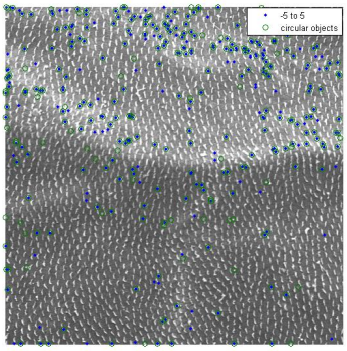

FIGURE 3.6: Object having near zero orientation and the circular ones are marked

3.4.2 Examining the effects of different shapes of objects

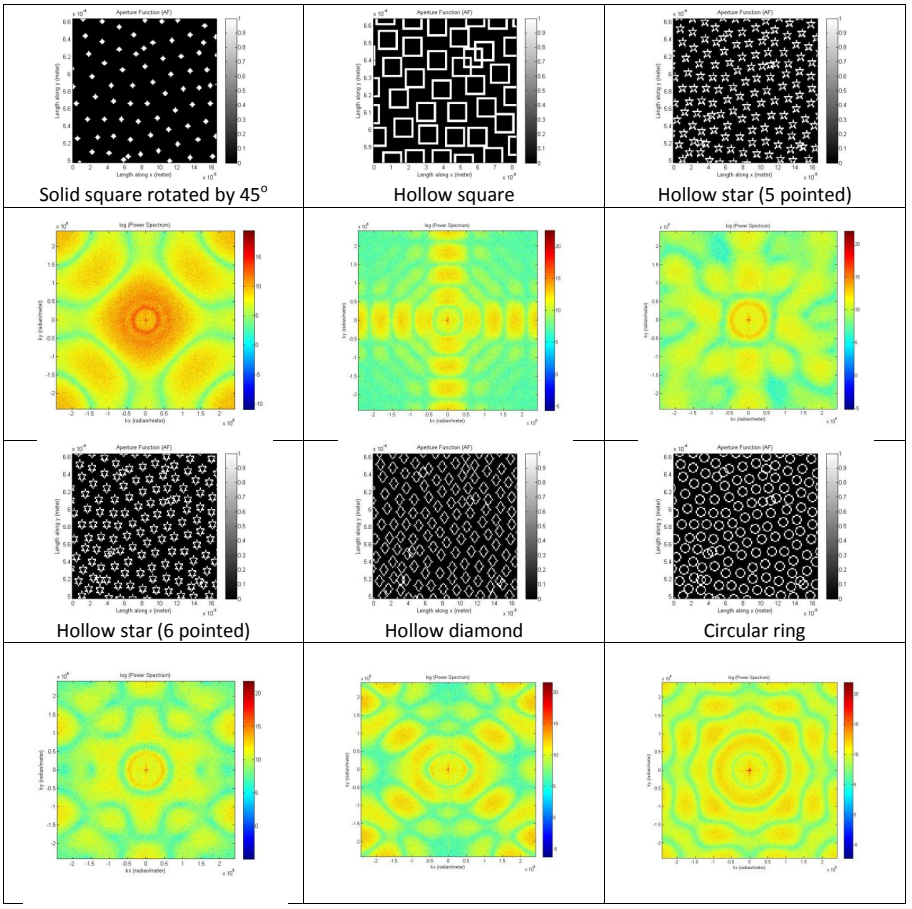

TABLE 3.4: Power spectra for various shapes on extracted coordinates (a)

This section presents the beautiful intensity distributions that appear when the extracted objects from the previous numerical experiment are replaced with identical shape objects such as rings, squares or triangles etc. The results are shown in Table 3.4 and 5.1 that clearly reflect the diversity as well as some common features in the power spectra for various shapes.

Chapter 4

Pattern generation

4.1 Introduction

This chapter is devoted to exploring the second approach of extracting information which is to develop a variety of 2D spatial arrangements of objects purely numerically that is used as a sample in the place of SEM image and then the power spectrum is calculated as before.

There are many logics for generating patterns. Simple as well as complex patterns can be generated via inbuilt functions for coordinate generation with a little bit of additional programming while patterns that emerge as a consequence of interaction among species, require solutions from non-trivial coupled system of partial differential equations with the recognition of valid parameter space among other models. I present insights from both of these methods emphasizing that generation of quasi periodic patterns can be done in infinite ways and a general, reduced and exhaustive scheme of its investigation is not yet available to my knowledge.

4.1.1 Pattern formation in biological systems

One can choose to generate patterns based on the mathematical models in the field of developmental biology under morphology to achieve or only explore a desired set of spatial wavelengths present in the system. This area is a complete field in itself and

several texts on the topic are available such as [9] and [10]. Solving these models is much more difficult than generating user defined patterns discussed in the next section because former must account for many interactions among components via linear or non-linear stability analyses of mostly the non-linear equations involved which the latter may skip and allocate a paticular object at a point purely for putting it there.

4.2 User defined pattern generation

4.2.1 2D analogue of N-slit experiment

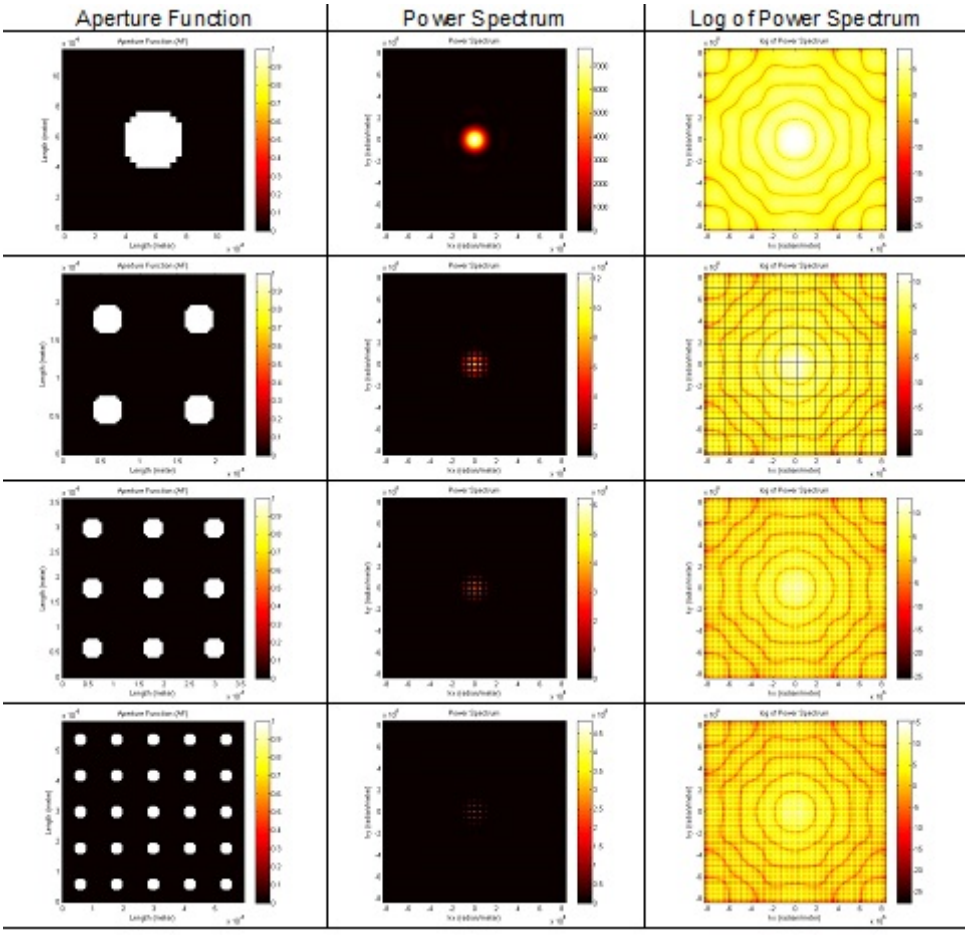

TABLE 4.1: 2D analogue of N-slit experiment

In first demonstration, I begin with an approximately circular aperture and approximate its observed diffraction pattern via power spectrum. Then, I increment the

number of apertures as an integer to the power two with identical spacing and shape to illustrate the 2D analogue of N-slit experiment. This illustration is given in Table 4.1.

4.2.2 Fluctuations in radius and center

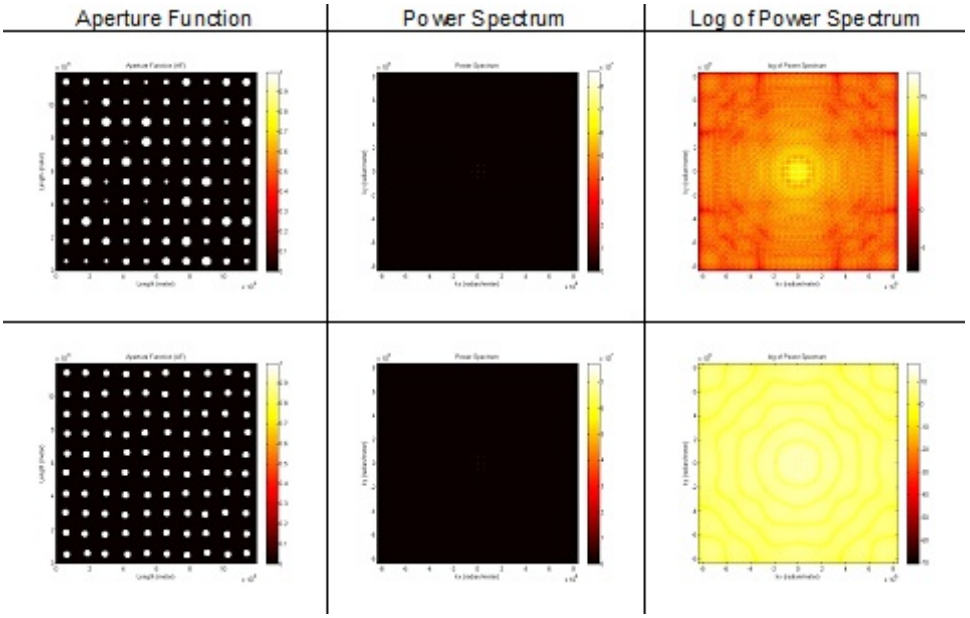

TABLE 4.2: Size distribution variation (first row) and interspacing distribution variation (second row); dx is 0.375μm

In the second demonstration, I introduce a size variation only in the radii of approximate circles by ±2dx using a uniform random distribution for 100 circle radii shown in first row of Table 4.2 and I introduce spacing variation from their centers ±2dx using a uniform random distribution for 100 circle centers shown in second row of Table 4.2. Please note that since the spaces are discrete, the radius or position random variable can now be found as any value from x, x+dx, x+2dx, x-dx or x-2dx if x is the mean value of that variable.

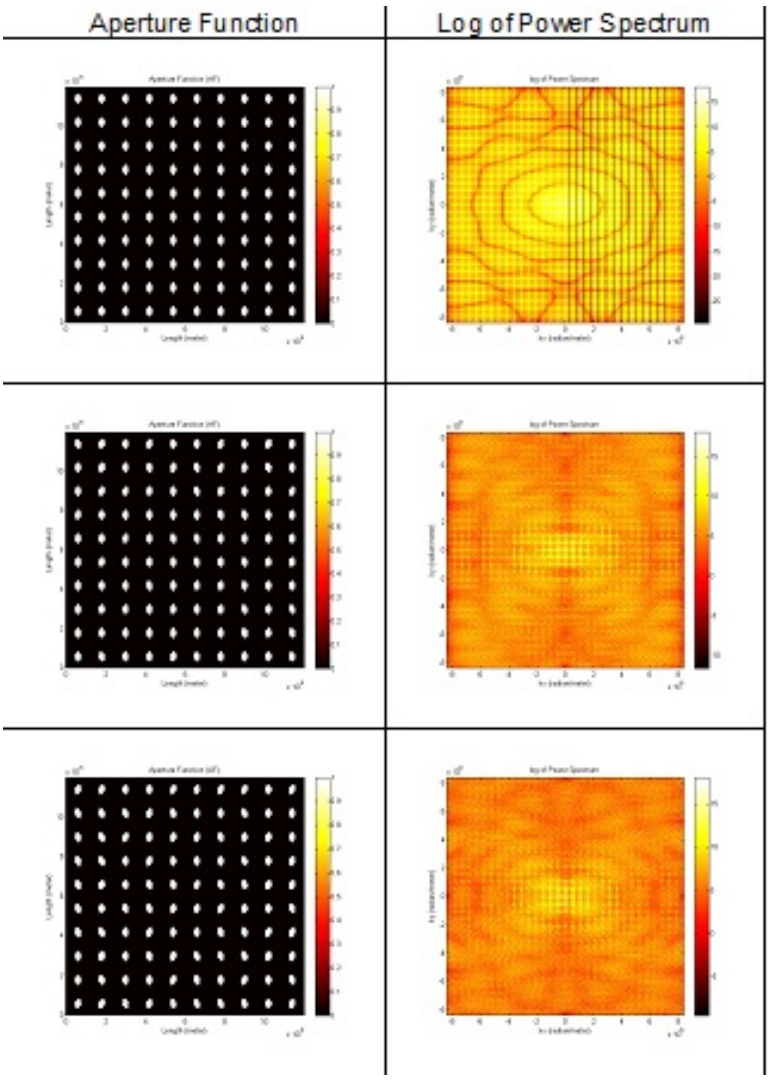

TABLE 4.3: Orientaion distribution variation. Ellipses at reference orientation (first row), ±10 degree variation (second row), ±20 degree variation (third row)

4.2.3 Fluctuations in orientation

In the third demonstration, I use ellipse for showing the effect of orientation distribution. In the Table 4.3, first row shows the arrangement of ellipses aligned with major axis along y axis, all in the same orientation. Second row is given ±10 degree variation about y axis. Third row is given ±20 degree variation about y axis. The variation is given in the same manner as before.

4.2.4 Multiple periodicities in one signal

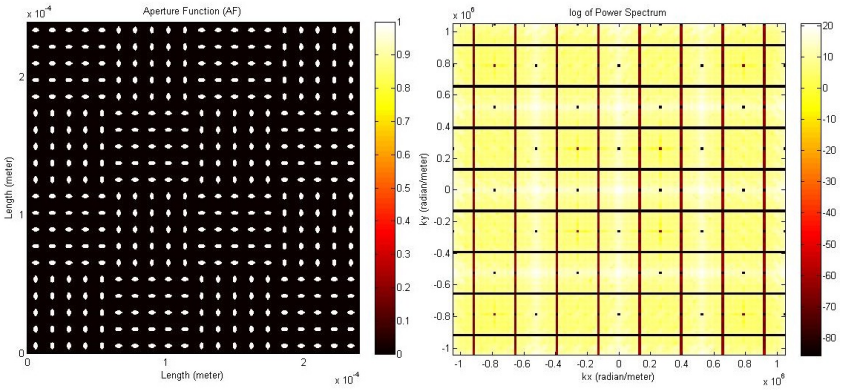

FIGURE 4.1: Many periodicities in one arrangement

In the fourth demonstration, I provide a perspective to understand the idea of having many kinds of periodicities in a single arrangement. This is the key explanation, though not a rigorous description of the various far-field intensity distributions discussed so far. I divide an array of 20X20 ellipses into a 4X4 array of 5X5 ellipses associated with each divided region and having a unique orientation for its ellipses. The arrangement shown in the left column of Figure 4.1 has periodically alternating orientation regions. Imagine a horizontal line crossing the vertically orientated major axis ellipses only; say it encounters an ellipse at every p unit. Move this line so that now it encounters the other orientation ellipses as well, so that it meets an ellipse at every q unit. Doing it over whole image gives only two such units p and q corresponding to which there must be peaks in the power spectrum. Obviously, peak corresponding to p will be less intense than that for q since q=2p in the shown image. Now, imagine a line parallel to the diagonal, this line encounters the ellipses with many different frequencies if it is moved parallel to itself. Another way is to consider the regions having same orientations for its ellipses as one unit and observe the periodicity of such units. The take-away point being that the power spectrum consists of peaks corresponding to all the periodicities in the arrangement. What happens, if periodicity is perturbed as in the second and third demonstration? The narrow peaks indicating high periodicity begin to spread depending upon the variables set to be perturbed. The final output is a result of all important variables that collectively define the 2D spatial arrangement and is hence complex.

Chapter 5

Concluding remarks

5.1 Summary and discussion

The complex spatial organization of the photonic elements referred to as 'objects' in this text constituting the biophotonic architecture can manipulate light in a variety of complex ways. A particular class of such behavior has been studied in detail via experimental and numerical methods in the form of multivariate analysis. Intensity distribution in the far-field or the power spectrum has been taken as the response variable while there are several input variables that collectively influence or control the response variable. One or more of the input variables have been varied while keeping the others constant to study the response variable.

In the first chapter, a glance at the diversity in the appearance of biophotonic architectures has been provided. Some of its biological functions for the species or its biomimetic applications have also been referred. The equivalence of the power spectrum calculated via the 2D FFT of an image of sample and the far-field optical diffraction pattern has been theoretically and visually elaborated, accounting the scaling terms. The agreement between the single wire optical diffraction pattern and the power spectrum of its image has been explicitly shown.

In the second chapter, I introduced the first hand observations for the particular problem that has been studied. Images of the sample at various magnifications ranging from 20x to 215x has been shown while SEM images of the sample at much higher resolution are also shown. The scattering patterns have been recorded for various variables external to the sample such as screen distance variation, beam spot size variation, beam spot position variation (over the sample) and laser source variation. Note that only one sample has been used which means the input variables that define the spatial pattern on the wing are unchanged. The key inferences from this chapter are as follows: Observed pattern is resolved by eyes when it is as close as 4 inch from the sample and then it only diverges away from the sample by around 2.26°. The scattering pattern does not look as it appears with a standard laser beam size of around 1-2 mm when a tightly focused beam spot is used. It begins to develop as the spot size is increased. When the beam spot was scanned over the wing, the pattern continuously changed its features in a non-linear way. Different laser sources were also used to qualitatively check wavelength sensitivity of the scattering pattern and it was observed that the red and green diode lasers gave very close patterns while that for a femto-second pulse contained additional features.

In the third chapter, I employed some numerical methods to extract information from the SEM image of the sample. I used morphological operations to change the structural input variables of the sample in a unique way that is not easily employed via other methods and its results were also interesting as some configurations gradually dissolved the side lobes leaving only the central spot while other configurations induced higher order lobes. I used image masking to simulate the effect of beam spot size regulation and showed much clearer results than those in the experiment. BLOB (binary or labeled objects) analysis gave the distributions of various geometric properties that have been presented as histograms or spatial distribution diagrams. The objects were modeled as ellipses for properties like orientation and length of axes. It was found that most frequent ranges for width were 2.5dx-3.5dx, for length were 8dx-9dx and for area were 16dx-17dx. For orientation, compared to other properties, a much smoother distribution with an angular deviation of $\pm 30°$ from the vertical axis of the image was present. Final section in this chapter presented a small numerical

experiment that shows beautiful power spectra that result when the extracted centroid coordinates are used to put identical shapes like rings, squares or triangles.

In the fourth chapter, I presented a numerical approach for generating the spatial pattern first, and then doing the power spectra calculation as before for various structural input variables. Firstly, I presented the 2D analogue of the N-slit experiment. Then I introduced small fluctuations ($\pm$2dx) in the radius and position of the center separately. Much stronger fluctuations ($\pm 10^\circ$ and $\pm$ 20°) for orientation have been shown. The corresponding power spectra have been shown for comparison. Finally, I explained the signatures of multiple periodicities present in the image into the Fourier space of power spectrum.

5.2 What more can be done

- One can use a variety of samples consisting of biophotonic architecture as I used only a termite wing. A similar or more advanced scheme of methods can be employed for classifying the biophotonic architectures into groups based on the response variable. An elaborate characterization of this particular complex optical behavior with the derivation of intrinsic structural variables composed of combinations of the presented varibales of this system in a mathematical model will be a fruitful study having a broad range of applications.

- Screen distance variation experiment: The Fresnel number is defined for a single element aperture not a complex aperture in my knowledge. The Fresnel number for an object of size $\sim 4\mu$m at green wavelength is $\sim 30\mu$m. For $\sim 10\mu$m it is $\sim 200\mu$m and for $\sim 50\mu$m it is $\sim$5mm. From the numerical results shown in section 3.3 it is clear that the pattern begins to develop at around the same diameter ($\sim 50\mu$m). We may consider this to be the effective diameter for the complex aperture function and then accordingly record intensity distributions in the range from zero to $\sim$5mm. So one can explore whether the scattering pattern develops after the Fresnel number (for complex aperture function) or

before it, that is in the near-field region. The side lobes before being resolved were possibly inside the bright region of the beam and may appear much before if a smaller beam radius is used.

- The extra information contained in the scattered pattern via femto-second pulses can make a good study.

- The numerical approach can be extended to much larger extent involving cluster analysis as one example or imposing various distributions like Gaussian, Possion or any arbitrary distribution to the objects' geometric properties discussed in section 3.4 or introducing varying disorder in the structural input variables and much more.

5.3 Possible applications of this study

Apart from the points mentioned in previous section which also serve as applications of methodology and results from this study for further research, there are some practical applications which are twofold. As the title says 'long range correlations', it simply means a measure of the correlated far-field optical diffraction pattern with respect to the spatial brightness distribution of optical field at the sample. The spatial frequency analysis methods (or simply the power spectra I used) are already employed in various studies in biophotonics [11], [12], [13] and biomedical imaging [14], [15]. If a theoretical model is proposed with relevant parameters as highlighted in the first point of previous section. It can have possible applications in optical probing of real time spatio-temporal changes at the mesoscopic scale which are of prime importance in many biomedical applications like tracking cell-differentiation where shape and size changes take place and physical applications like designing photonic waveguides, regulation of element size in photonic crystal manufacturing. Such ideas can be conceived in reference to the power spectra shown in Table 3.1 and 5.1.

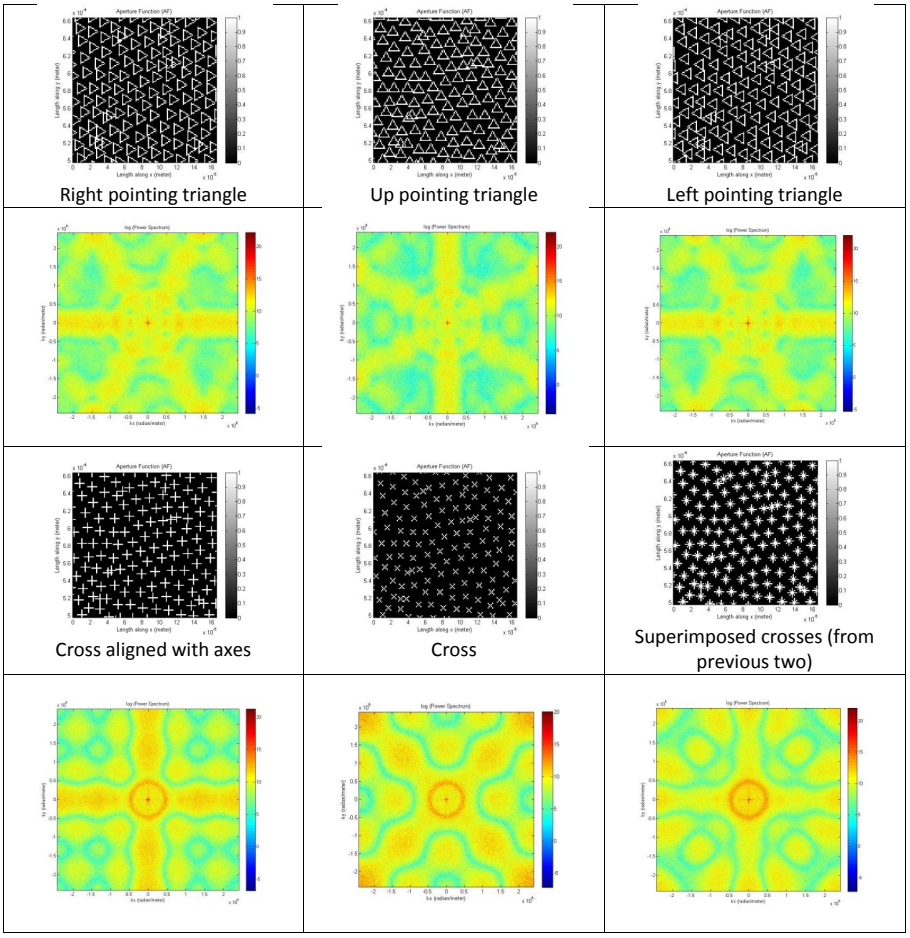

TABLE 5.1: Power spectra for various shapes on extracted coordinates (b)

Appendix A

MATLAB scripts

The details of the specific uses of commands and functions can be found in the MATLAB documentation and it must be noted that some experience in programming is required for using this code as it will be required to replace some symbols from multiple locations to appropriately run it. Another important point regarding calculation of power spectra is the transform length, that must be increased to atleast twice the size of sample image. I used MATLAB version 7.6.0.324 (R2008a).

A.1 For SEM image analysis

```
clear
% number of pixels to square crop the image file
n=512;
% read the image file here
cima=im2double(imread(image filename));
% set crop limits here
cima=imcrop(cima,[1 1 511 511]);
% adjust background illumination if it is non uniform
bkgrnd=imopen(cima,strel('disk',3));
I3=imadjust(imsubtract(cima,bkgrnd));
% create a binary image here
level = graythresh(I3);
```

```
bw =im2bw(I3,level);
% label or identify the objects here
[labeled,numObjects] = bwlabel(bw,8);
% calculate various geometric properties of the identified objects here
graindata = regionprops(labeled,'Area','Centroid','Orientation','MajorAxis
Length','MinorAxisLength');


% create separate easy to use variables from the above data structure of prop-
erties
for k=1:numObjects
xx(k,:)=[graindata(k,1).Centroid(1,1)+(0.5*graindata(k,1).MajorAxisLength(1,1)
*cos(deg2rad(graindata(k,1).Orientation(1,1))))...
graindata(k,1).Centroid(1,1)-(0.5*graindata(k,1).MajorAxisLength(1,1)
*cos(deg2rad(graindata(k,1).Orientation(1,1))))];
yy(k,:)=[graindata(k,1).Centroid(1,2)+(0.5*graindata(k,1).MajorAxisLength(1,1)
*sin(deg2rad(graindata(k,1).Orientation(1,1))))...
graindata(k,1).Centroid(1,2)-(0.5*graindata(k,1).MajorAxisLength(1,1)
*sin(deg2rad(graindata(k,1).Orientation(1,1))))];
x(k,1)=graindata(k,1).Centroid(1,1);
y(k,1)=graindata(k,1).Centroid(1,2);
end


for i=1:numObjects
A(i)=graindata(i,1).Area(1,1);
O(i)=graindata(i,1).Orientation(1,1);
M(i)=graindata(i,1).MajorAxisLength(1,1);
m(i)=graindata(i,1).MinorAxisLength(1,1);
end
```

A.2 For pattern generation

```
clear
Ncellmax=20;%#of cells along 1 direction
pxprcell=32;acell=12e-6;%#of pix per cell and square cell parameter
N=Ncellmax*pxprcell;%#of grid pts
dx=acell/pxprcell;dy=acell/pxprcell;%smallest length element


%minor rectangular grid for each cell
xcell=dx*[0:pxprcell-1];ycell=dy*[0:pxprcell-1];
cellcntrx=.5*[max(xcell)-min(xcell)];cellcntry=.5*[max(ycell)-min(ycell)];
[xcell ycell]=meshgrid(xcell,ycell);


a=3e-6;b=5e-6;%a=width along x; b=length along y or length of arc (for curved
structure)
%r1=ri*1e-6;%inner radius for curved structure
zo=cellcntrx+i*cellcntry;%complex notation
[t r]=cart2pol(xcell-cellcntrx,ycell-cellcntrx);z=r.*exp(i*t);%minor grid in polar
co-ords.


%fluctuation amplitudes
sigma_int_angle=0;%individual orientation
sigma_int_fl_x=0;sigma_int_fl_y=0;%individual positional
sigma_fl_a=0;sigma_fl_b=0;sigma_fl_r1=0;%individual size/shape


%-----------------------------------------------------------
%fluctuation distribution for each cell based on fluctuation amplitudes


%rotang=round(sigma_int_angle*(rand(Ncellmax)-.5))+(0);
%rotang=repmat(-15:30/(Ncellmax-1):15,Ncellmax,1)+rotang;
%rotang=repmat([235 125;-235 -125],Ncellmax/2,Ncellmax/2);
%rotang=cat(1,repmat(180:-180/((Ncellmax-1)):0,Ncellmax/2,1),
```

```
repmat(-180:180/((Ncellmax-1)):0,Ncellmax/2,1))+rotang;%non random distri-
bution for orientation


fl_x=dx*round(sigma_int_fl_x*(rand(Ncellmax)-.5));
fl_y=dy*round(sigma_int_fl_y*(rand(Ncellmax)-.5));
fl_a=dx*round(sigma_fl_a*(rand(Ncellmax)-.5));
fl_b=dy*round(sigma_fl_b*(rand(Ncellmax)-.5));
fl_z=fl_x+i*fl_y;fl_r1=dx*round(sigma_fl_r1*(rand(Ncellmax)-.5));


%Wavy pattern and other non random distributions————————————
%[zx,zy]=meshgrid(-4*pi:8*pi/(Ncellmax-1):4*pi,-4*pi:8*pi/(Ncellmax-1):4*pi);
%fl_z=cat(1,repmat((-1:2/(Ncellmax-1):1).*3e-6,Ncellmax/2,1),
repmat((1:-2/(Ncellmax-1):-1).*3e-6,Ncellmax/2,1));fl_z=fl_z';
%fl_z1=((cos(4*zy)+i*sin(9*zx)).*1e-6);fl_z2=((cos(9*zy)+i*sin(4*zx)).*1e-6);
%fl_z=cat(2,fl_z1(1:Ncellmax,1:(Ncellmax/4)),
fl_z2(1:Ncellmax,(Ncellmax/4)+1:Ncellmax/2),...
% fl_z1(1:Ncellmax,(Ncellmax/2)+1:(3*Ncellmax/4)),
fl_z2(1:Ncellmax,(3*Ncellmax/4)+1:Ncellmax));


%fl_z=repmat([-3 ;3],Ncellmax/2,Ncellmax).*1e-6 + fl_z;
% sigma_int_angle_patch=180;Npatchmax=4;cellprpatch=Ncellmax/Npatchmax;
% rotang_patch_mag=round(sigma_int_angle_patch*(rand(Npatchmax)-.5));
%for u=1:Npatchmax
% for v=1:Npatchmax
% rotang_patch((u-1)*cellprpatch+[1:cellprpatch],(v-1)
cellprpatch+[1:cellprpatch])=rotang_patch_mag(u,v);
% end
%end


%Shape selection and aperture function————————————————————-
f = zeros(N,N);
for u=1:Ncellmax
for v=1:Ncellmax
```

```
%Gaussian
%fcell=exp(- (( ( (xcell-(cellcntrx+fl_x(v,u)))/...
% ((((a/2)+fl_a(u,v)))) ).power2 +...
% ( (ycell-(cellcntry+fl_y(v,u)) )/...
% ((((b/2)+fl_b(u,v)))) ).power2 ) ));


%circle
fcell = ( ((xcell-(cellcntrx+fl_x(v,u)) )/((a/2)+fl_a(u,v))).power2 +
((ycell-(cellcntry+fl_y(v,u)) )/((b/2)+fl_b(u,v))).power2¡=1);
%rectangle
%fcell = ((xcell-(cellcntrx+fl_x(v,u)))¡=(a+fl_a(u,v))/2 &
(xcell-(cellcntrx+fl_x(v,u)))¿=(-a+fl_a(u,v))/2 &
(ycell-(cellcntry+fl_y(v,u)))¡=(b+fl_b(u,v))/2 &
(ycell-(cellcntry+fl_y(v,u)))¿=(-b+fl_b(u,v))/2);
%triangle
%fcell = ((xcell-(cellcntrx+fl_x(v,u)))/(a+fl_a(u,v)) +
(ycell-(cellcntry+fl_y(v,u)))/(b+fl_b(u,v)) ¡=1 &
(xcell-(cellcntrx+fl_x(v,u)))¿=0 &
(ycell-(cellcntry+fl_y(v,u)))¿=0);
%Curved structure
%theta=(b+fl_b(u,v))/(r1+fl_r1(u,v)+(a+fl_a(u,v))/2);
%fcell=(abs(z+r1+fl_z(v,u))¡=(a+fl_a(u,v))+r1+fl_r1(u,v) & ...
% abs(z+r1+fl_z(v,u))¿=r1+fl_r1(u,v) & ...
% angle(z+r1+fl_z(v,u))¿-theta/2 & angle(z+r1+fl_z(v,u))¡theta/2);


%theta=(b+fl_b(u,v))/(r1+(a+fl_a(u,v))/2);
%fcell=( exp(- ( ((r-r1)/(.5*(a+fl_a(u,v)))).power2 ) ));
% .*exp(-(((t-0)/(.5*(pi/3))).power2)));
%rotang(v,u)=round((rand-.5)*rotang_patch(v,u));


%Symmetry operation (rotation) over each cell————————————
fcell = imrotate(fcell,rotang(v,u),'crop');
```

```
f((v-1)*pxprcell+[1:pxprcell],(u-1)*pxprcell+[1:pxprcell]) = fcell;
end
end
%Symmetry operation over selected regions----------------------------
%f1=imrotate(f(1:N/2,1:N/2),3,'crop');
f4=imrotate(f(N/2+1:N,N/2+1:N),15,'crop');
%f3=imrotate(f(N/2+1:N,1:N/2),-15,'crop');
f2=imrotate(f(1:N/2,N/2+1:N),9,'crop');
%fo=imrotate(f1(1:N/4,1:N/4),3,'crop');
f1(1:N/4,1:N/4)=fo;
fo=imrotate(f2(1:N/4,1:N/4),3,'crop');
f2(1:N/4,1:N/4)=fo;
%f=[f1 f2;f3 f4];


%Background noise and final surface modulation / masking
%f=imnoise(f,'gaussian',0,.009);


%[X Y]=meshgrid(dx*(0:N-1),dx*(0:N-1));
%Z=exp(- (( ( (X-(N*dx/2))/...
% (((br))) ).power2 +...
% ( (Y-(N*dx/2))/...
% (((br))) ).power2 )) );f=f.*Z; % Gaussian Signal Final Modulation
%Z=(((X-(N*dx/2))./(N*dx/4)).power2+((Y-(N*dx/2))./(N*dx/4)).power2¿=1
& ((X-(N*dx/2))./(N*dx/2)).power2+((Y-(N*dx/2))./(N*dx/2)).power2¡=1);
%Z=(((X-(N*dx/2))./(br)).power2+((Y-(N*dx/2))./(br)).power2¿=1);
%f=f.*Z;


%Reults-------------------------------------------------------------
tl=1024;%length of transform length
%fCor=corr(f);%pairwise correlation
fr = fftshift(fft2(f,tl,tl));% frMod =(fr.*conj(fr));%power spectrum
frPhase =angle(fr);
xxx=(0:N-1)*(dx);zzz=(-tl/2:tl/2-1)*(2*pi/(tl*dx));
```

```
%subplot(1,3,1),%set(gcf,'windowstyle','docked')
figure,imagesc([xxx(1) xxx(N)],[xxx(1) xxx(N)],f),colormap(hot),axis xy square,...
xlabel('Length (meter)'),ylabel('Length (meter)'),title('Aperture Function (AF)'),
colorbar%[1 1 1;0 0 0]
%figure,imagesc([xxx(1) xxx(N)],[xxx(1) xxx(N)],fCor),colormap(jet),
axis xy square,...
% xlabel('Length (meter)'),ylabel('Length (meter)'),title('Correlation Matrix for
AF'),
colorbar%[1 1 1;0 0 0]
%subplot(1,3,2)
%figure,imagesc([zzz(1) zzz(tl)],[zzz(1) zzz(tl)],(frMod)),colormap(hot),axis xy
square,...
% xlabel('kx (radian/meter)'),ylabel('ky (radian/meter)'),title('Power Spectrum'),
colorbar%,axis([-2e6 2e6 -2e6 2e6])
%subplot(1,3,3)
figure,imagesc([zzz(1) zzz(tl)],[zzz(1) zzz(tl)],log(frMod)),colormap(hot),axis xy
square,...
xlabel('kx (radian/meter)'),ylabel('ky (radian/meter)'),title('log of Power Spec-
trum'),
colorbar%,axis([-2e6 2e6 -2e6 2e6])
```

Bibliography

[1] L. P. et al Bir. Quasi-ordered photonic bandgap materials of biologic origin: butterfly scales. *Proc. SPIE*, 6593:659318–659318–8, 2007. doi: 10.1117/12.723535. URL http://dx.doi.org/10.1117/12.723535.

[2] Pramod Kumar, Danish Shamoon, Dhirendra P. Singh, Sudip Mandal, and Kamal P. Singh. Unveiling spatial correlations in biophotonic architectures of transparent insect wings. *Proceedings of International Conference on Photonics, Optics and Laser technology*, 2013. doi: 10.5220/0004339001060110.

[3] C. Pouya, D. G. Stavenga, and P. Vukusic. Discovery of ordered and quasi-ordered photonic crystal structures in the scales of the beetle eupholus magnificus. *Opt. Express*, 19(12):11355–11364, Jun 2011. doi: 10.1364/OE.19.011355. URL http://www.opticsexpress.org/abstract.cfm?URI=oe-19-12-11355.

[4] E. Shevtsova et al. Stable structural color patterns displayed on transparent insect wings. *PNAS*, pages 668–673, November 2011. URL www.pnas.org/cgi/doi/10.1073/pnas.1017393108.

[5] P. Vukusic and J.R. Sambles. Photonic structures in biology. *Nature*, 424:852–855, August 2003. URL doi:10.1038/nature01941.

[6] Nathan F Lepora, Paul Verschure, and Tony J Prescott. The state of the art in biomimetics. *Bioinspiration and Biomimetics*, 8(1):013001, 2013. URL http://stacks.iop.org/1748-3190/8/i=1/a=013001.

[7] F. Martin and C. Aime. Some spectral properties of random arrays of grains. *J. Opt. Soc. Am.*, 69(9):1315–1320, Sep 1979. doi: 10.1364/JOSA.

69.001315. URL http://www.opticsinfobase.org/abstract.cfm?URI=josa-69-9-1315.

[8] Pramod Kumar, Danish Shamoon, Dhirendra P. Singh, Sudip Mandal, and Kamal P. Singh. Optical probing of long range spatial correlation and symmetry in complex biophotonic architectures in the transparent insect wings. May 2013. URL arXiv:1305.2097v1.

[9] J D Murray. *Mathematical Biology*. Springer, third edition.

[10] Leah Edelstein-Keshet. *Mathematical models in Biology*. SIAM, first edition.

[11] K. Kertsz et al. Photonic band gap materials in butterfly scales: A possible source of blueprints. *Materials Science and Engineering: B*, 149(3): 259 – 265, 2008. ISSN 0921-5107. doi: http://dx.doi.org/10.1016/j.mseb.2007.10.013. URL http://www.sciencedirect.com/science/article/pii/S0921510707005971.

[12] Pramod Kumar, Danish Shamoon, and Kamal P. Singh. Optical functionality of natural photonic structures on the transparent insect wings for bio-mimetic applications. *Proc. SPIE*, 9056:90561L–90561L–9, 2014. doi: 10.1117/12.2044867. URL http://dx.doi.org/10.1117/12.2044867.

[13] Pramod Kumar, Danish Shamoon, and Kamal P. Singh. Probing spatiotemporal optical complex functionality of photonic systems. *Workshop on Recent Advances in Photonics*, December 2013.

[14] Steve Bégin. Local assessment of myelin health in a multiple sclerosis mouse model using a 2d fourier transform approach. *Biomed. Opt. Express*, 4(10): 2003–2014, Oct 2013. doi: 10.1364/BOE.4.002003. URL http://www.opticsinfobase.org/boe/abstract.cfm?URI=boe-4-10-2003.

[15] Pu Y. et al. Spatial frequency analysis for detecting early stage of cancer in human cervical tissues. *Technol Cancer Res Treat.*, 2013. doi: 10.7785/tcrtexpress.2013.600270.